The Synergetic Ionic and Electronic Features of $MAPbI_3$ Perovskite Films Revealed by Electrochemical Impedance Spectroscopy

*Sauraj Jha, Ross Haroldson, Anvar A. Zakhidov, and Jason D. Slinker**

Dr. S. Jha, Prof. A. A. Zakhidov, Prof. J. D. Slinker
Department of Materials Science and Engineering
The University of Texas at Dallas
800 West Campbell Road, SCI 10, Richardson, Texas 75080-3021, United States
E-mail: slinker@utdallas.edu

Dr. R. Haroldson, Prof. A. A. Zakhidov, Prof. J. D. Slinker
Department of Physics
The University of Texas at Dallas
800 West Campbell Road, SCI 10, Richardson, Texas 75080-3021, United States

Prof. J. D. Slinker
Department of Chemistry
The University of Texas at Dallas
800 West Campbell Road, SCI 10, Richardson, Texas 75080-3021, United States

Prof. A. A. Zakhidov
NanoTech Institute, The University of Texas at Dallas, 800 West Campbell Road, Richardson, Texas 75080-3021, United States.

Keywords: cyclic voltammetry, methylammonium lead iodide, electrochemistry, degradation, hydrofluoroether

Perovskites have emerged as a forerunner of electronics research due to their vast potential for optoelectronic applications. The numerous combinations of constituent ions and the potential for doping of perovskites lead to a high demand to track the underlying electronic properties. Solution-based electrochemistry is particularly promising for detailed and facile assessment of perovskites. Here, we perform electrochemical impedance spectroscopy (EIS) of $MAPbI_3$ thin films and model them with an equivalent circuit that accounts for solvent, ionic, and thin film effects. A dielectric constant consistent with prior ac studies and a diffusion constant harmonious with cation motion in $MAPbI_3$ were extracted. An electrical double layer thickness in the perovskite film of 54 nm was obtained, consistent with lithium doping in perovskite films. Comparing the EIS and equivalent circuit model of perovskite films to control ITO-only data enabled the assignment of the ions at each interface. This comparison implied a double layer of primarily lithium ions inside

the perovskite film at the solution interface with significant recombination of ions on the solution side of the interface. This demonstrates EIS as a powerful tool for studying the fundamental charge accumulation and transport processes in perovskite thin films.

1. Introduction

Perovskites are at the forefront of optoelectronics research as solution-cast crystalline semiconductors with high mobility and tunable properties.[1] Hybrid metal-halide perovskites have emerged for solar applications due to observations of high power conversion efficiencies from the advantageous properties of organic and inorganic semiconducting components.[2] These hybrid perovskites offer modular interchange of the constituent ions and unique charge carrier dynamics. Ultimately, rational optimization of hybrid perovskites necessitates understanding the interplay of the factors contributing to ionic and electronic conduction in thin films of these materials.

Solution-based electrochemistry is a facile benchtop method for accessing the electronic states and ionic contributions of semiconducting and mixed conducting materials and systems.[3] However, hybrid metal-halide perovskites are particularly challenging to assess by solution-based electrochemistry, as most aqueous and organic electrolyte solutions will dissolve the film and destroy the advantageous crystalline structure.[4] Recently, electrochemical approaches have been developed to assess perovskite thin films under various liquid electrolytes.[5] Of these electrochemistry techniques, some have found utility with hybrid metal-halide perovskite thin films for assessing energy levels and doping with lithium.[5c, 5d, 5f-h] One predominant approach utilizes a modular solvent toolkit based on hydrofluoroethers (HFEs).[5f, 5h] HFEs behave as an "orthogonal solvent," interfacing with organic, inorganic, and hybrid electronic materials with minimal to no degradation.[6] The HFE solvent toolkit was demonstrated as a promising nondestructive approach for characterizing and processing perovskite thin films specifically prepared for solar applications.

Here, we utilize the HFE solvent toolkit to perform electrochemical impedance spectroscopy (EIS) of a methylammonium lead iodide $MAPbI_3$ thin film and fit the results with equivalent circuit modeling. While this method has been applied to complete solid-state photovoltaic devices,[7] this approach has yet to be applied under solution-based electrochemistry of perovskite films. Distinct features of electrolyte solution, ions, and perovskite film features are

processes are identified. Controls are performed to validate associated circuit elements and assign ions at the interfaces. The implications are discussed for understanding and optimizing devices.

2. Results and Discussion

2.1. EIS of $MAPbI_3$ in HFE

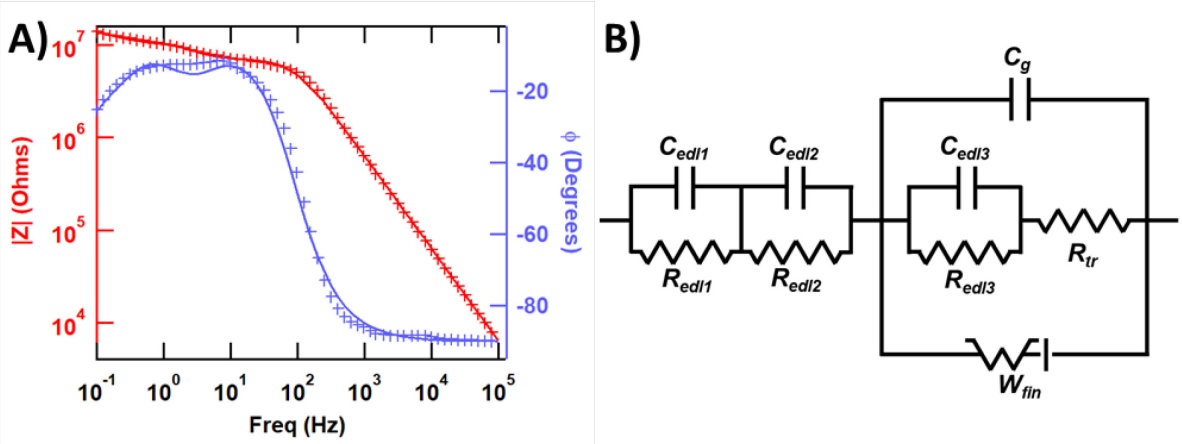

Figure 1. (A) EIS of a $MAPbI_3$ thin film on an ITO electrode in HFE electrolyte. (B) Equivalent circuit model for a $MAPbI_3$ thin film on an ITO electrode in HFE electrolyte. *Edl1* is associated with Li^+ ions at the Pt wire counter electrode. *Edl2* is associated with PF_6^- ions in solution at the solution/perovskite interface, and *edl3* is associated with Li^+ ions in the perovskite film at the solution/perovskite interface. C_g is the geometric capacitance of the perovskite film. W_{fin} is a finite Warburg diffusion element, and R_{tr} is the transient resistance to traverse the film.

EIS was first performed on a ~350 nm thick $MAPbI_3$ thin film on an ITO electrode in HFE electrolyte (95% HFE, 5% DEC v/v, 0.1 M $LiPF_6$). Example SEM images, film photographs, and photoluminescence spectra are shown in Figure S1-S3, Supporting Information. The resulting data for the complex impedance is shown in Figure 1A. The complex impedance is represented as:

$$Z(\omega) = |Z(\omega)|e^{i\phi(\omega)} \quad (1)$$

where $|Z(\omega)|$ is the magnitude or modulus of the impedance, and $\varphi(\omega)$ is the phase. The ac frequency was swept from 1 MHz to 0.1 Hz. The resulting plots of the complex impedance

magnitude and phase are nontrivial given the many dynamics that can transpire in the electrolyte solution and perovskite thin film. To accurately fit these curves, we employed an equivalent circuit model, as shown in Figure 1B. This circuit was rationalized as a series of parallel RC elements (R_{edl1}, C_{edl1}; R_{edl2}, C_{edl2}) in series with a three-forked parallel circuit bearing two capacitors (C_g, C_{edl3}), two resistors (R_{edl3} and R_{tr}) and one finite Warburg diffusion element (W_{fin}).

The parallel RC circuit elements can be rationalized as the solution and double-layer formation at the reference electrode and perovskite thin film interface. C_g is understood as the geometric capacitance of the perovskite thin film. C_{edl3} and R_{edl3} are due to double-layer formation in the $MAPbI_3$ thin film. R_{tr} is the transient resistance to traverse the film, and the Warburg element accounts for diffusion in the perovskite film. The p-value of the χ^2 goodness of fit test for this sample was 0.00172, indicating agreement with the specified set.

This measurement was repeated over seven independent electrodes from four independent films, thus incorporating variations both across films and across sample preparations. The χ^2 goodness of fit test for all samples was less than 0.05 for all fits with the equivalent circuit model of Figure 1B, indicating consistent behavior and broad application of this model. The geometric mean of each circuit element is shown in Table 1. A plot of these values, together with the range of geometric standard error of the distributions, is shown in Figure 2.

Table 1. Geometric mean values of the circuit elements from fitting EIS data for $MAPbI_3$ films in HFE electrolyte. *Edl1* is associated with Li^+ ions at the Pt wire counter electrode. *Edl2* is associated with PF_6^- ions in solution at the solution/perovskite interface, and *edl3* is associated with Li^+ ions in the perovskite film at the solution/perovskite interface.

R_{edl1} [MΩ]	C_{edl1} [nF]	R_{edl2} [MΩ]	C_{edl2} [nF]	R_{edl3} [MΩ]	C_{edl3} [nF]	C_g [nF]	R_{tr} [kΩ]	A_w [nS·s$^{-1/2}$]	B [s$^{1/2}$]
16	290	0.73	0.22	19	179	28	60	180	4.0

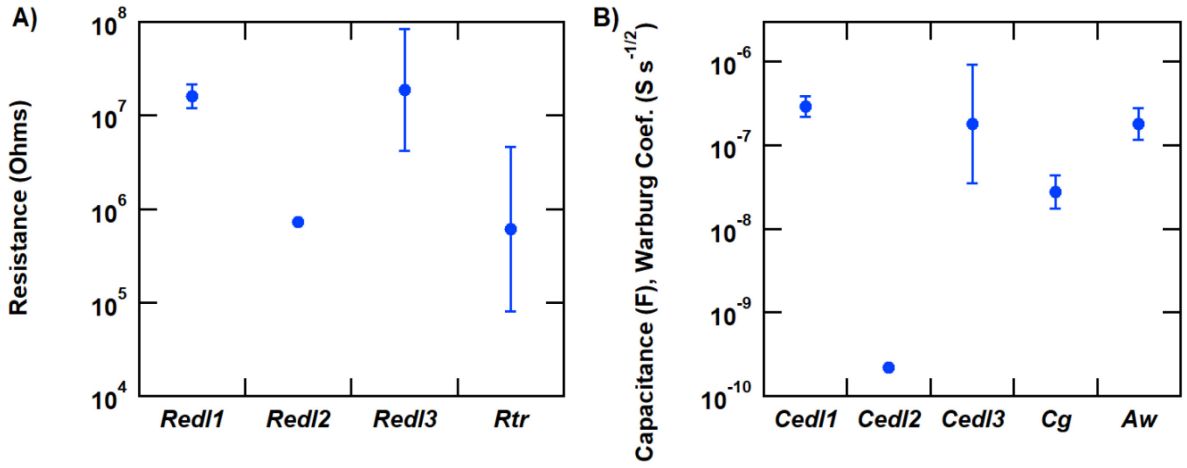

Figure 2. Geometric mean values of the circuit elements from fitting EIS data for $MAPbI_3$ films on ITO in HFE electrolyte. Error bars represent the range spanned by the geometric standard error of each. (A) Geometric mean values of the resistive circuit elements. (B) Geometric mean values of the capacitive and the Warburg coefficient.

The complex impedance of the finite Warburg diffusion element is represented by:

$$Z_{W_{fin}}(\omega) = \frac{A_W}{\sqrt{i\omega}} coth\left(B\sqrt{i\omega}\right) \qquad (2)$$

where A_w is the Warburg coefficient and B is a factor equal to:

$$B = \frac{\delta}{\sqrt{D}} = 4.0 \overset{\times}{\div} 1.5 \qquad (3)$$

where δ is the thickness of the diffusion layer, D is the diffusion coefficient, and the values are the geometric mean with the geometric standard error. Assuming the diffusion layer thickness is the thickness of the perovskite film, an apparent D of 8×10^{-11} cm^2 s^{-1} is obtained, which falls within the values reported for ion diffusion in $MAPbI_3$ films.[8]

The dielectric constant ε_R of the perovskite film can be extracted from the geometric capacitance C_g by:

$$\varepsilon_R = \frac{C_g d}{\epsilon_0 A} \qquad (4)$$

where d is the device thickness (~350 nm), A is the electrode area (2.0 mm^2), and ε_0 is the permittivity of free space (8.85 × 10^{-12} F/m). A dielectric constant of 540 is obtained using these values. The dielectric constants of perovskites such as $MAPbI_3$ are highly frequency dependent,[9] and our extracted value is consistent with others in the low-frequency range (~1 Hz).[9a-c] Subsequently, assuming that the dielectric constant is uniform through the perovskite film, the apparent electric double layer thickness d_{edl3} can be extracted:

$$C_g d = \varepsilon_R \varepsilon_0 A = C_{edl3} d_{edl3} \quad (5)$$

From Equation 5, d_{edl3} = 54 nm is obtained, yielding a relative width of d_{edl3}/d = 0.15. This ratio is within the range of values reported for variable $LiPF_6$ doping in $CsPbBr_3$ thin films, correlating to a mole ratio of 0.056 lithium salt in the perovskite matrix.[10]

2.2. EIS of ITO control in HFE

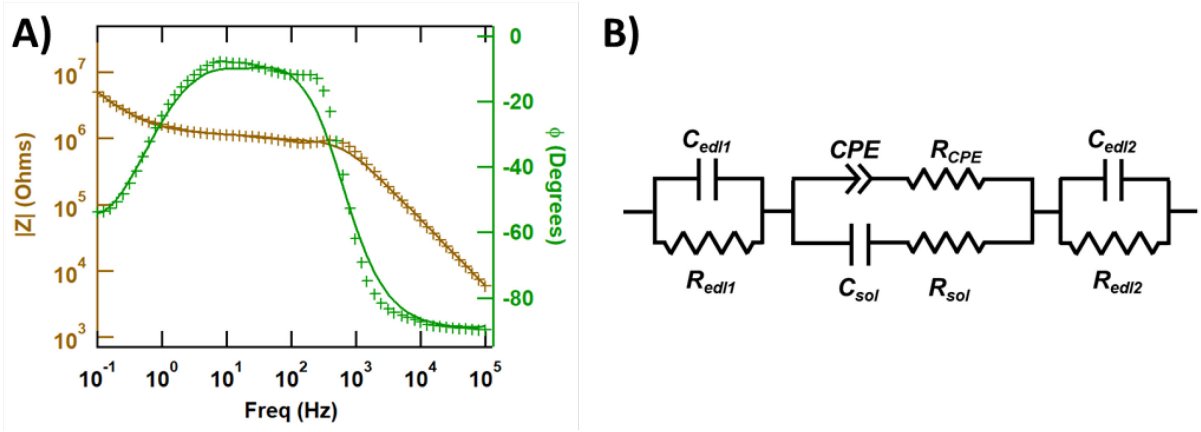

Figure 3. (A) EIS of an ITO film in HFE electrolyte. (B) Equivalent circuit model for an ITO electrode in HFE electrolyte. *Edl1* is associated with Li^+ ions at the Pt wire counter electrode. *Edl2* is associated with PF_6^- ions in solution at the solution/perovskite interface, *sol* elements are associated with the bulk solution, *CPE* is a constant phase element, and R_{CPE} is the real resistance associated with the CPE.

To verify this model and understanding of the solution and thin film components of the EIS model for the $MAPbI_3$ film electrochemistry, we ran a control with the same solution components but no perovskite film on the ITO. The complex impedance from a representative sample for this situation

is shown in Figure 3. An equivalent circuit was found that provided an accurate fitting for this and across three additional measurements (χ^2 goodness of fit < 0.01 for all samples). This equivalent circuit exhibited similar series of parallel RC elements (R_{edl1}, C_{edl1}; R_{edl2}, C_{edl2}) in series with to a two-forked circuit, with one fork consisting of a resistor (R_{CPE}) and a constant phase element (CPE) and the other fork composed of a resistor (R_{sol}) and capacitor (C_{sol}) in series. The geometric means of these fit parameters across four samples are given in Table 2, with the values plotted along with geometric standard errors in Figure 4.

The constant phase element has a complex impedance of:

$$Z_{CPE}(\omega) = \frac{1}{A_{cpe}(i\omega)^{\alpha}} \quad (3)$$

where A_{cpe} is the constant phase element coefficient and α is an exponent ranging from −1 to 1.

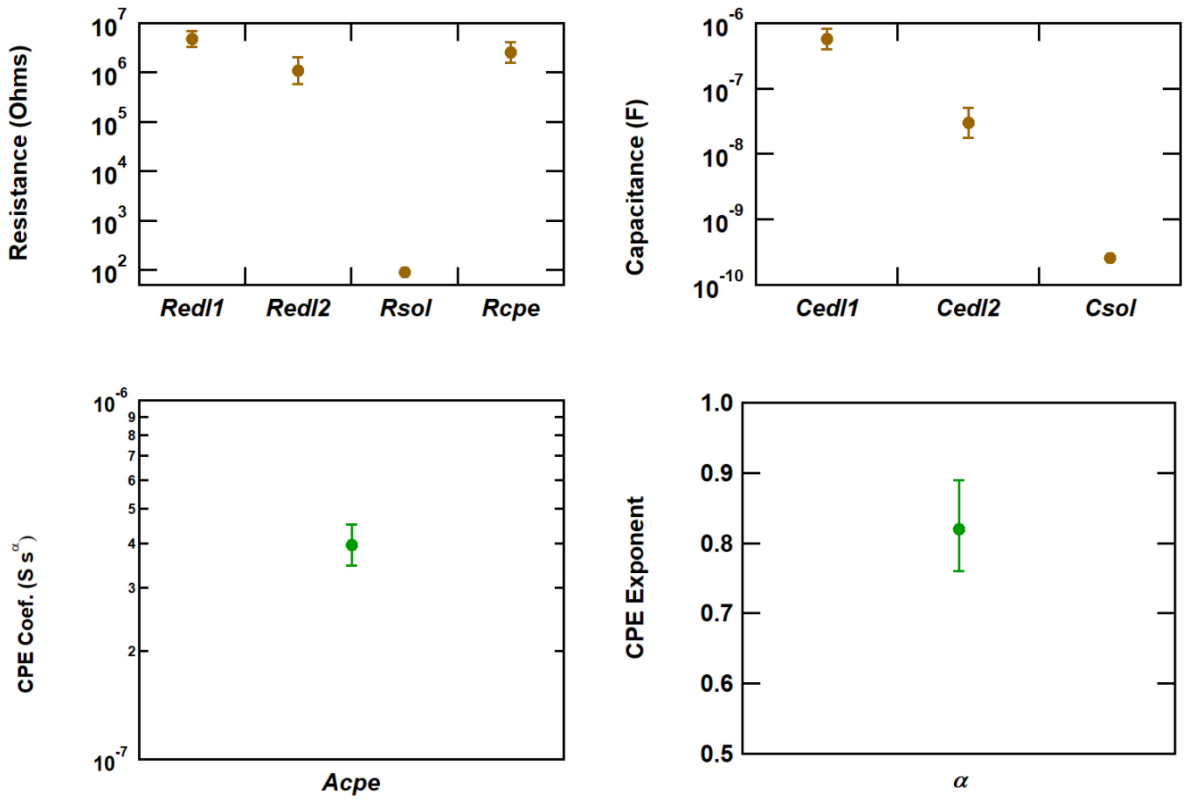

Figure 4. Geometric mean values of the circuit elements from fitting EIS data for an ITO film in HFE electrolyte. Error bars represent the range spanned by the geometric standard error of each.

Table 2. Geometric mean values of the circuit elements from fitting EIS data for ITO films in HFE electrolyte. *Edl1* is associated with PF_6^- ions at the Pt wire counter electrode. *Edl2* is associated with Li^+ ions in solution at the solution/perovskite interface, W_{fin} is a finite Warburg diffusion element, *CPE* is a constant phase element, and R_{CPE} is the real resistance associated with the *CPE*.

R_{edl1} [MΩ]	C_{edl1} [nF]	R_{edl2} [MΩ]	C_{edl2} [nF]	R_{CPE} [MΩ]	R_{sol} [Ω]	C_{sol} [pF]	A_{cpe} [nS·α]	α
4.9	580	1.1	30	2.5	91	260	390	0.82

Importantly, while the values for R_{edl1}, C_{edl1}, R_{edl2}, and C_{edl2} are similar to those found for the perovskite film case, they possess key differences that can be utilized to gain greater insight. In particular, a detailed look into the capacitance at each interface for the case of the ITO-only film electrochemistry can be used to reveal the identities of the ions accumulating at each electrode. First, for EDL formation at the ITO electrode or ITO/perovskite electrode, we assume a parallel plate capacitor with a dielectric and that the radius of the ion r_{ion} sets the effective width,

$$C_{ITO,edl} = \epsilon_R \epsilon_0 \frac{A_{ITO}}{r_{ion}} \quad (6)$$

Then, for the platinum wire counter electrode, we assume a cylindrical capacitor with plate separation of the radius of the ion, plus the parallel plate contribution from the end cap:

$$C_{Pt,edl} = 2\pi\epsilon_R \epsilon_0 \frac{L_{Pt}}{\ln\left[(r_{Pt}+r_{ion})/r_{Pt}\right]} + \epsilon_R \epsilon_0 \frac{A_{Pt}}{r_{ion}} \quad (7)$$

where L_{Pt} and r_{Pt} are the exposed length and the radius of the Pt wire counter electrode. This enables the identification of the ion type at each electrode from the ratios of the EDL capacitances:

$$\frac{C_{Pt,PF_6}}{C_{ITO,Li}} = 1.8 \text{ and } \frac{C_{Pt,Li}}{C_{ITO,PF_6}} = 24 \quad (8)$$

For the ITO-only case, C_{edl1}/C_{edl2} = 19, suggesting that Li^+ ions are accumulating at the platinum electrode that PF_6^- ions are accumulating at the ITO (**Figure 5**). For the perovskite film, C_{edl1} is comparable to the ITO-only case, but C_{edl2} drops precipitously for the perovskite film case. While the specific numbers leave some room for debate, let us assume that the similar C_{edl1} values mean that Li^+ ions are still accumulating at the Pt counter electrode. Under this view, the lowered

magnitude of C_{edl2} follows from the recombination of PF_6^- with positive ions such as inherent MA^+ or Li^+ dopants from the film. This is consistent with our prior observation of precipitates on the surface of the perovskite film after electrochemical driving[5h] and following HFE electrolyte exposure (Figure S2). This assertion, plus the details of the d_{edl3} and the propensity for lithium doping in $MAPbI_3$, are consistent with a double layer of primarily Li^+ in the perovskite film constituting *edl3* (Figure 5).

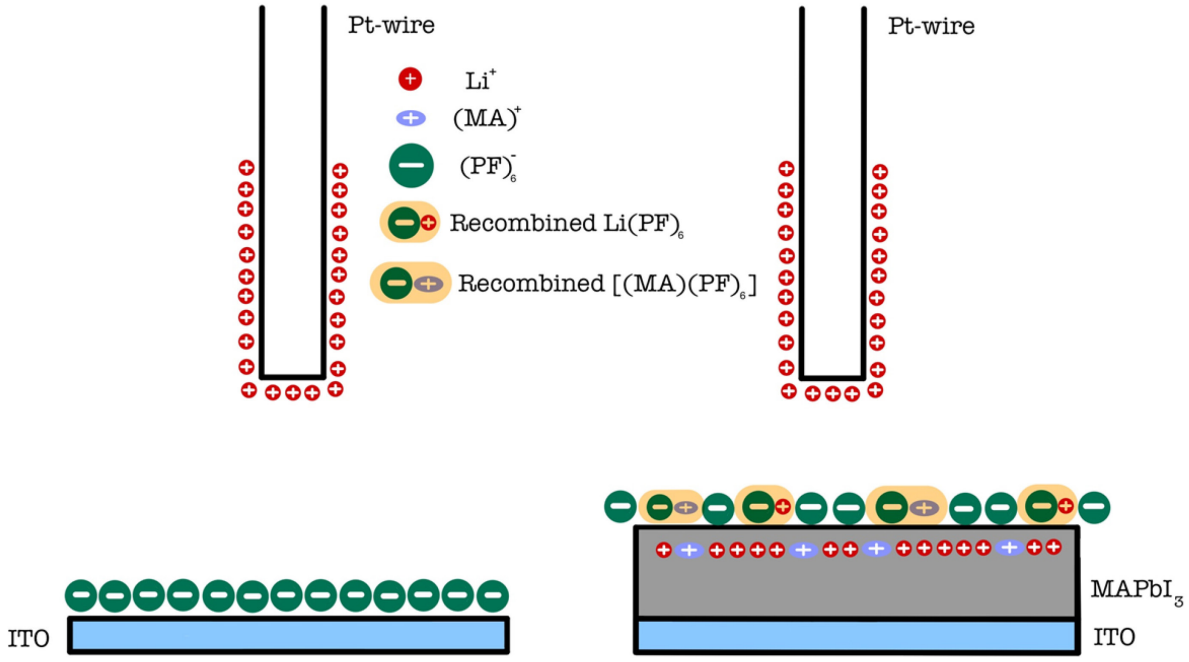

Figure 5. Illustration of the ion accumulation at the interfaces for ITO and $MAPbI_3$ on ITO films in HFE solutions.

The other circuit elements for the ITO-only model are then associated with the bulk solution and the thin film interfaces. Without the thin film present, the low capacitance (C_{sol}) and low resistance (R_{sol}) associated with the electrolyte solution is apparent. For the CPE, the alpha value near one suggests this circuit element acts approximately as a capacitor. CPEs are common in mixed conducting systems, where inhomogeneous dynamics can lead to time-broadened processes.[11]

3. Conclusion

EIS was performed on a $MAPbI_3$ thin film with an HFE electrolyte solution. An equivalent circuit model was identified that fit across 7 distinct measurements (χ^2 p-value < 0.05). The model was rationalized in terms of electrolyte solution and perovskite film components, and circuit parameters were extracted. A dielectric constant consistent with ac perovskite studies and a diffustion constant consistent with cation motion was extracted for the $MAPbI_3$ film. An electrical double layer thickness in the perovskite film of 54 nm was found, a relative thickness consistent with lithium doping in perovskite films. A control experiment in HFE electrolyte solution on an ITO electrode without the perovskite film showed a similar solution electrical double-layer components and required fewer circuit elements to fit. This control experiment accomplished the assignment of the EDLs to particular interfaces and ions. This demonstrates EIS as a powerful tool for studying the fundamental charge accumulation and transport processes in perovskite thin films.

4. Materials and Methods

4.1. Perovskite Ink Solution Preparation

A 1:1:1 molar ratio, 1 M perovskite ink of lead iodide, methylammonium acetate, and methylammonium iodide was prepared as described previously.[28] Lead (II) iodide (Tokyo Chemical Industry, 99.99%) was dissolved in anhydrous N, N-dimethylformamide (Sigma-Aldrich, 99.8%) by stirring at 700 rpm at 70 °C for 30 mins followed by room-temperature addition and stirring of methylammonium iodide (Lumtec, 99.5%) and methylammonium acetate (Greatcell Solar Materials), respectively. The solution was stirred for one hour and was filtered using a nylon syringe filter (0.22 μm pore size, Aireka Cells) immediately before spin coating.

4.2. Device Fabrication

Prepatterned ITO/glass substrates (150 nm, ~20 Ω sq^{-1}) bearing sixteen circular 2 mm^2 electrodes were purchased from Thin Film Devices, Inc. These slides were cleaned in a sequence of non-ionic detergent wash, water bath sonication, and UV ozone treatment. The filtered perovskite ink was dispensed at the center of the substrate and was spin-cast with a 5 s ramp time and 60 s spin duration followed by 100 °C annealing for 10 mins.

4.3. Electrochemical Testing

A three-electrode configuration was used for electrochemical measurements with a 2.0 mm non-aqueous no-leak Ag/AgCl reference electrode (eDAQ, Inc.) and a 0.5 mm diameter platinum wire as a counter electrode. The electrolyte was prepared by dissolving 0.1 M $LiPF_6$ (battery grade, ≥ 99.99% trace metals basis) in diethyl carbonate (DEC, anhydrous, ≥ 99%, Sigma-Aldrich). The mixture was then added to a HFE solvent (3M Novec 7500, 3-Ethoxyperfluoro(2-methylhexane)) that had been previously degassed by bubbling argon gas for 60 mins. Electrochemical impedance spectroscopy measurements were performed on a vibration isolation table using a CHI750D Electrochemical Analyzer and a CHI684 multiplexer in a Faraday cage and under an argon atmosphere. Films were measured in the dark. EIS was performed at 0 V vs. Ag/AgCl reference electrode and a 5 mV amplitude.

Supporting Information

Supporting information is available from the Wiley Online Library or from the author.

Acknowledgements

J.D.S. acknowledges support from the National Science Foundation (ECCS 1906505). A.Z. acknowledges support from the Welch Foundation (AT-1617) and the Russian Science Foundation (19-73-30023).

Conflict of Interest

The authors declare no conflict of interest.

Data Availability

The data that support the findings of this study are available from the corresponding author upon reasonable request.

Received: ((will be filled in by the editorial staff))

Revised: ((will be filled in by the editorial staff))

Published online: ((will be filled in by the editorial staff))

References

[1] a) J. Y. Kim, J.-W. Lee, H. S. Jung, H. Shin, N.-G. Park, *Chem. Rev.* **2020**, *120*, 7867-7918; b) J. Jeong, M. Kim, J. Seo, H. Lu, P. Ahlawat, A. Mishra, Y. Yang, M. A. Hope, F. T. Eickemeyer, M. Kim, Y. J. Yoon, I. W. Choi, B. P. Darwich, S. J. Choi, Y. Jo, J. H. Lee, B. Walker, S. M. Zakeeruddin, L. Emsley, U. Rothlisberger, A. Hagfeldt, D. S. Kim, M. Grätzel, J. Y. Kim, *Nature* **2021**, *592*, 381-385; c) Y.-H. Kim, S. Kim, A. Kakekhani, J. Park, J. Park, Y.-H. Lee, H. Xu, S. Nagane, R. B. Wexler, D.-H. Kim, S. H. Jo, L. Martínez-Sarti, P. Tan, A. Sadhanala, G.-S. Park, Y.-W. Kim, B. Hu, H. J. Bolink, S. Yoo, R. H. Friend, A. M. Rappe, T.-W. Lee, *Nat. Photonics* **2021**, *15*, 148-155; d) D. Ma, K. Lin, Y. Dong, H. Choubisa, A. H. Proppe, D. Wu, Y.-K. Wang, B. Chen, P. Li, J. Z. Fan, F. Yuan, A. Johnston, Y. Liu, Y. Kang, Z.-H. Lu, Z. Wei, E. H. Sargent, *Nature* **2021**, *599*, 594-598; e) D. W. Zhao, C. Chen, C. L. Wang, M. M. Junda, Z. N. Song, C. R. Grice, Y. Yu, C. W. Li, B. Subedi, N. J. Podraza, X. Z. Zhao, G. J. Fang, R. G. Xiong, K. Zhu, Y. F. Yan, *Nat. Energy* **2018**, *3*, 1093-1100; f) C. Wehrenfennig, G. E. Eperon, M. B. Johnston, H. J. Snaith, L. M. Herz, *Adv. Mater.* **2014**, *26*, 1584-1589; g) C. S. Ponseca, T. J. Savenije, M. Abdellah, K. B. Zheng, A. Yartsev, T. Pascher, T. Harlang, P. Chabera, T. Pullerits, A. Stepanov, J. P. Wolf, V. Sundstrom, *J. Am. Chem. Soc.* **2014**, *136*, 5189-5192; h) L. Protesescu, S. Yakunin, M. I. Bodnarchuk, F. Krieg, R. Caputo, C. H. Hendon, R. X. Yang, A. Walsh, M. V. Kovalenko, *Nano Lett.* **2015**, *15*, 3692-3696; i) N. Yantara, S. Bhaumik, F. Yan, D. Sabba, H. A. Dewi, N. Mathews, P. P. Boix, H. V. Demir, S. Mhaisalkar, *J. Phys. Chem. Lett.* **2015**, *6*, 4360-4364; j) X. Li, Y. Wu, S. Zhang, B. Cai, Y. Gu, J. Song, H. Zeng, *Adv. Funct. Mater.* **2016**, *26*, 2435-2445; k) G. Li, F. W. R. Rivarola, N. J. L. K. Davis, S. Bai, T. C. Jellicoe, F. de la Peña, S. Hou, C. Ducati, F. Gao, R. H. Friend, N. C. Greenham, Z.-K. Tan, *Adv. Mater.* **2016**, *28*, 3528-3534.

[2] a) S. Brittman, G. W. P. Adhyaksa, E. C. Garnett, *MRS Commun.* **2015**, *5*, 7-26; b) K. Leng, W. Fu, Y. Liu, M. Chhowalla, K. P. Loh, *Nat. Rev. Mater.* **2020**, *5*, 482-500; c) H. L. B. Boström, A. L. Goodwin, *Accounts Chem. Res.* **2021**, *54*, 1288-1297; d) K. Frohna, S. D. Stranks, in *Handbook of Organic Materials for Electronic and Photonic Devices (Second Edition)* (Ed.: O. Ostroverkhova), Woodhead Publishing, **2019**, pp. 211-256; e)

K. Sakhatskyi, R. A. John, A. Guerrero, S. Tsarev, S. Sabisch, T. Das, G. J. Matt, S. Yakunin, I. Cherniukh, M. Kotyrba, Y. Berezovska, M. I. Bodnarchuk, S. Chakraborty, J. Bisquert, M. V. Kovalenko, *ACS Energy Letters* **2022**, *7*, 3401-3414.

[3] a) H. J. Lewerenz, *Chem. Soc. Rev.* **1997**, *26*, 239-246; b) V. A. Myamlin, V. P. Yurii, *Russ. Chem. Rev.* **1963**, *32*, 207; c) B. Zhu, L. Fan, N. Mushtaq, R. Raza, M. Sajid, Y. Wu, W. Lin, J.-S. Kim, P. D. Lund, S. Yun, *Electrochem. Energy Rev.* **2021**, *4*, 757-792.

[4] a) B. J. Kim, D. H. Kim, S. Kwon, S. Park, Z. Li, K. Zhu, H. Jung, *Nat. Commun.* **2016**, *7*, 11735; b) E. Greul, P. Docampo, T. Bein, *Z. Anorg. Allg. Chem* **2017**, *643*, 1704-1711.

[5] a) Q. L. Jiang, M. M. Chen, J. Q. Li, M. C. Wang, X. Q. Zeng, T. Besara, J. Lu, Y. Xin, X. Shan, B. C. Pan, C. C. Wang, S. C. Lin, T. Siegrist, Q. F. Xiao, Z. B. Yu, *ACS Nano* **2017**, *11*, 1073-1079; b) Q. Jiang, X. Zeng, N. Wang, Z. Xiao, Z. Guo, J. Lu, *ACS Energy Lett.* **2018**, *3*, 264-269; c) J. A. Dawson, A. J. Naylor, C. Eames, M. Roberts, W. Zhang, H. J. Snaith, P. G. Bruce, M. S. Islam, *ACS Energy Lett.* **2017**, *2*, 1818-1824; d) N. Vicente, G. Garcia-Belmonte, *J. Phys. Chem. Lett.* **2017**, *8*, 1371-1374; e) J. T. Mulder, I. du Fosse, M. A. Jazi, L. Manna, A. J. Houtepen, *ACS Energy Lett.* **2021**, *6*, 2519-2525; f) M. Hasan, S. Venkatesan, D. Lyashenko, J. D. Slinker, A. Zakhidov, *Anal. Chem.* **2017**, *89*, 9649-9653; g) G. F. Samu, R. A. Scheidt, P. V. Kamat, C. Janáky, *Chem. Mat.* **2018**, *30*, 561-569; h) S. Jha, M. Hasan, N. Khakurel, C. A. Ryan, R. McMullen, A. Mishra, A. V. Malko, A. A. Zakhidov, J. D. Slinker, *Mater. Today Adv.* **2022**, *13*, 100213; i) D. Moia, I. Gelmetti, P. Calado, W. Fisher, M. Stringer, O. Game, Y. Hu, P. Docampo, D. Lidzey, E. Palomares, J. Nelson, P. R. F. Barnes, *Energy Environ. Sci.* **2019**, *12*, 1296-1308.

[6] a) A. A. Zakhidov, S. Reineke, B. Lüssem, K. Leo, *Org. Electron.* **2012**, *13*, 356-360; b) A. A. Zakhidov, J.-K. Lee, H. H. Fong, J. A. DeFranco, M. Chatzichristidi, P. G. Taylor, C. K. Ober, G. G. Malliaras, *Adv. Mater.* **2008**, *20*, 3481-3484; c) A. A. Zakhidov, J. K. Lee, J. A. DeFranco, H. H. Fong, P. G. Taylor, M. Chatzichristidi, C. K. Ober, G. G. Malliaras, *Chem. Sci* **2011**, *2*, 1178-1182.

[7] a) E. Ghahremanirad, O. Almora, S. Suresh, A. A. Drew, T. H. Chowdhury, A. R. Uhl, *Adv. Energy Mater.* **2023**, *13*, 2204370; b) A. Guerrero, J. Bisquert, G. Garcia-Belmonte, *Chem. Rev.* **2021**, *121*, 14430-14484.

[8] M. H. Futscher, J. M. Lee, L. McGovern, L. A. Muscarella, T. Y. Wang, M. I. Haider, A. Fakharuddin, L. Schmidt-Mende, B. Ehrler, *Mater. Horizons* **2019**, *6*, 1497-1503.

[9] a) M. Sajedi Alvar, P. W. M. Blom, G.-J. A. H. Wetzelaer, *Adv. Electron. Mater.* **2020**, *6*, 1900935; b) M. N. F. Hoque, M. Yang, Z. Li, N. Islam, X. Pan, K. Zhu, Z. Fan, *ACS Energy Lett.* **2016**, *1*, 142-149; c) E. J. Juarez-Perez, R. S. Sanchez, L. Badia, G. Garcia-Belmonte, Y. S. Kang, I. Mora-Sero, J. Bisquert, *J. Phys. Chem. Lett.* **2014**, *5*, 2390-2394; d) S. Govinda, B. P. Kore, M. Bokdam, P. Mahale, A. Kumar, S. Pal, B. Bhattacharyya, J. Lahnsteiner, G. Kresse, C. Franchini, A. Pandey, D. D. Sarma, *J Phys Chem Lett* **2017**, *8*, 4113-4121.

[10] A. Mishra, M. Alahbakhshi, R. Haroldson, L. D. Bastatas, Q. Gu, A. A. Zakhidov, J. D. Slinker, *Adv. Opt. Mater.* **2020**, *8*, 2000226.

[11] a) S. Kochowski, K. Nitsch, *Thin Solid Films* **2002**, *415*, 133-137; b) A. Lasia, *J. Phys. Chem. Lett.* **2022**, *13*, 580-589.

Perovskites offer rich underlying physics due to the interplay of electronic and ionic effects. However, accessing the details of these interactions is challenging due to the fragility of perovskite films. Here, we utilize electrochemical impedance spectroscopy with a hydrofluoroether solvent toolkit to identify ion identities, quantify double layer formation, and estimate the dielectric constants of $MAPbI_3$ films.

Sauraj Jha, Ross Haroldson, Anvar A. Zakhidov, and Jason D. Slinker

The Synergetic Ionic and Electronic Features of $MAPbI_3$ Perovskite Films Revealed by Electrochemical Impedance Spectroscopy

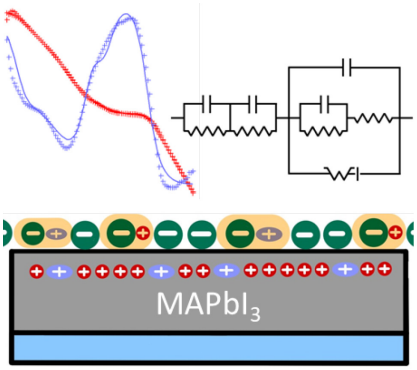

Supporting Information

The Synergetic Ionic and Electronic Features of $MAPbI_3$ Perovskite Films Revealed by Electrochemical Impedance Spectroscopy

Sauraj Jha, Ross Haroldson, Anvar A. Zakhidov, and Jason D. Slinker

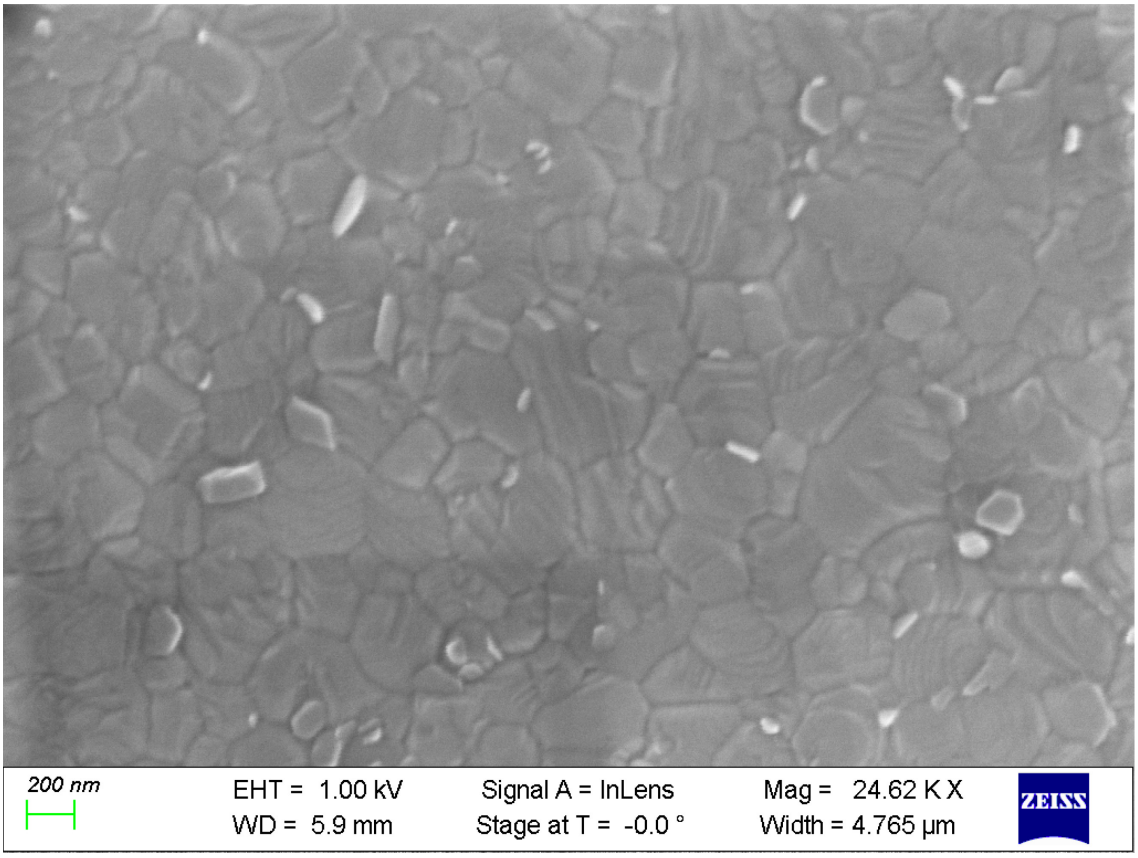

Figure S1. Scanning electron microscopy (SEM) image of a prepared $MAPbI_3$ thin film.

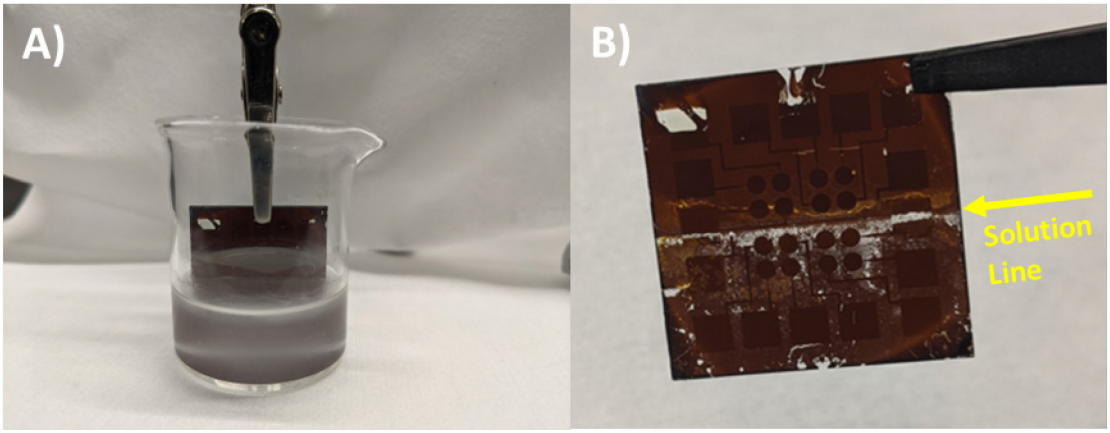

Figure S2. Exposure of a $MAPbI_3$ film to the hydrofluoroether (HFE) electrolyte (95% 3M Novec 7500 HFE, 5% diethyl carbonate v/v, 0.1 M $LiPF_6$) solution. A) Photograph of a $MAPbI_3$ film on an ITO/glass substrate being dipped in the electrolyte. B) Photograph of a $MAPbI_3$ film exposed on the lower half to the HFE electrolyte for 5 min. Note the salt deposits are particularly apparent along the solution exposure line.

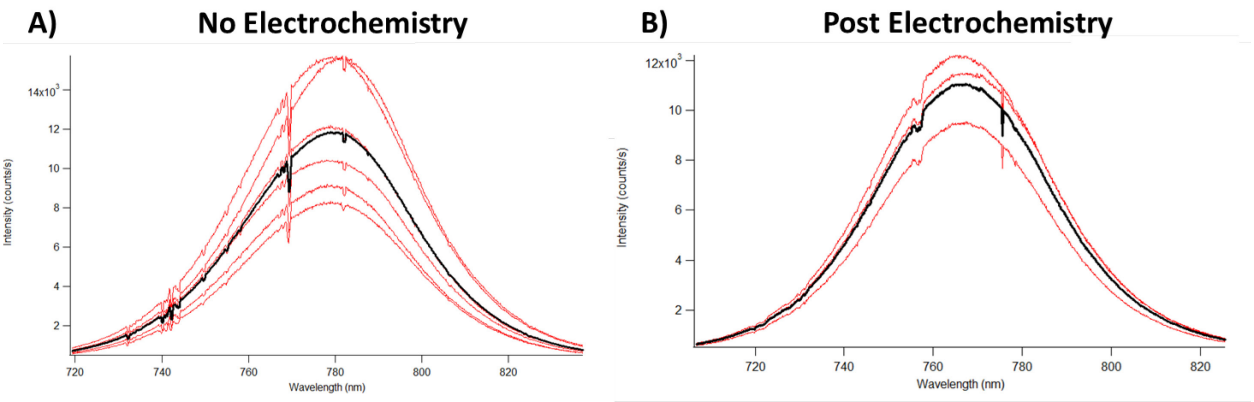

Figure S3. Photoluminescence spectra of $MAPbI_3$ films before and after electrochemical testing in an HFE electrolyte. Several spectra are shown for each film for points taken on the electrode surface, and the black curves are the averages of these curves. There is no apparent change in the shape of the spectra between the films.